PHYSICAL REVIEW D **78,** 074011 (2008)

QCD corrections to polarization of J/ψ and Υ at Fermilab Tevatron and CERN LHC

Bin Gong and Jian-Xiong Wang

Institute of High Energy Physics, Chinese Academy of Sciences, P.O. Box 918(4), Beijing, 100049, China
and Theoretical Physics Center for Science Facilities, Beijing, 100049, China

(Received 19 May 2008; revised manuscript received 5 August 2008; published 10 October 2008)

In this work, we present more details of the calculation on the next-to-leading-order (NLO) QCD corrections to polarization of direct J/ψ production via color singlet at the Tevatron and LHC, together with the results for Υ for the first time. Our results show that the J/ψ polarization status drastically changes from transverse polarization dominant at leading order into longitudinal polarization dominant in the whole range of the transverse momentum p_t of J/ψ when the NLO corrections are counted. For Υ production, the p_t distribution of the polarization status behaves almost the same as that for J/ψ except that the NLO result is transverse polarization at small p_t range. Although the theoretical evaluation predicts a larger longitudinal polarization than the measured value at the Tevatron, it may provide a solution towards the previous large discrepancy for J/ψ and Υ polarization between theoretical prediction and experimental measurement, and suggests that the next important step is to calculate the NLO corrections to hadronproduction of color-octet state $J/\psi^{(8)}$ and $\Upsilon^{(8)}$. Our calculations are performed in two ways: namely, we do and do not analytically sum over the polarizations, and then check them with each other.

DOI: 10.1103/PhysRevD.78.074011 PACS numbers: 12.38.Bx, 13.25.Gv, 13.60.Le

I. INTRODUCTION

The study of J/ψ production in various experiments is a very interesting topic since its discovery in 1974. It is a good place to probe both perturbative and nonperturbative aspects of QCD dynamics. To describe the huge discrepancy of the high-p_t J/ψ production between the theoretical calculation based on the color-singlet mechanism [1] and the experimental measurement by the CDF Collaboration at the Tevatron [2], the color-octet mechanism [3] was proposed based on the nonrelativistic QCD (NRQCD) [4]. The factorization formalism of NRQCD provides a theoretical framework to the treatment of heavy-quarkonium production. It allows consistent theoretical prediction to be made and to be improved systematically in the QCD coupling constant α_s and the heavy-quark relative velocity v. The color-singlet mechanism is straightforward from the perturbative QCD, but the color-octet mechanism depends on nonperturbative universal NRQCD matrix elements. So various efforts have been made to confirm this mechanism, or to fix the magnitudes of the universal NRQCD matrix elements. Although it seems to show qualitative agreements with experimental data, there are certain difficulties in the quantitative estimate in NRQCD for J/ψ photoproduction at the DESY ep collider HERA [5–10], $J/\psi(\psi')$ and Υ polarization of hadronproduction at the Fermilab Tevatron, and J/ψ production at B-factories. A review of the situation can be found in Ref. [11].

Without next-to-leading-order (NLO) corrections, it is difficult to obtain agreement between the experimental results and leading-order theoretical predictions for J/ψ production. There are a few examples that NLO corrections are quite large. It was found that the current experimental results on inelastic J/ψ photoproduction [12,13] are adequately described by the color-singlet channel alone once higher-order QCD corrections are included [7,8], although Ref. [14] found that the DELPHI [15] data evidently favor the NRQCD formalism for J/ψ production, $\gamma + \gamma \to J/\psi + X$, rather than the color-singlet model. And it was also found in Ref. [16] that the QCD higher-order process $\gamma + \gamma \to J/\psi + c + \bar{c}$ gives the same order and even larger contribution at high p_t than the leading-order color-singlet processes. In Ref. [17], the NLO process $c + g \to J/\psi + c$, where the initial c quark is the intrinsic c quark from the proton at the Tevatron, gives larger contribution at high p_t than the leading-order color-singlet processes. The large discrepancies found in the single and double charmonium production in e^+e^- annihilation at B-factories between LO theoretical predictions [18–20] and experimental results [21,22] were studied in many works. It seems that they may be resolved by including higher-order correction: NLO QCD and relativistic corrections [18,23–28].

Based on NRQCD, the LO calculation predicts a sizable transverse polarization for J/ψ production at high p_t at the Tevatron [29–31] while the measurement at the Fermilab Tevatron [32] gives a slight longitudinal polarized result. In a recent paper [33], the measurement on polarization of Υ production at the Tevatron is presented and the NRQCD prediction [34] does not coincide with it. Beyond the NRQCD framework, there is an attempt by using s-channel treatment to J/ψ hadronproduction in the work of Ref. [35], which gives longitudinal polarization. Within the NRQCD framework, to calculate higher-order corrections is an important step towards the solution of such puzzles. Recently, NLO QCD corrections to J/ψ hadron-

production have been calculated in Ref. [36]. The results show that the total cross section is boosted by a factor of about 2 and the J/ψ transverse momentum p_t distribution is enhanced more and more as p_t becomes larger. A real correction process $g + g \to J/\psi + c + \bar{c}$ at NLO, which is not included in Ref. [36], was calculated in [16,37]. It gives sizable contribution to p_t distribution of J/ψ at the high p_t region, and it alone gives an almost unpolarized result. Therefore it is very interesting to know the result of J/ψ polarization when NLO QCD corrections are included. In a recent paper [38], we presented a calculation on the NLO QCD corrections to the J/ψ polarization in hadronproduction at the Tevatron and LHC. In this paper, we give more details of the calculation, and the results for Υ polarization for the first time. The results show that the polarizations of J/ψ and Υ are drastically changed from more transverse polarization at LO into more longitudinal polarization at NLO. Meanwhile, our results for total cross section and transverse momentum distribution are consistent with Ref. [36]. In this calculation, we use our Feynman Diagram Calculation package (FDC) [39] with a newly added part of a complete set of methods to calculate tensor and scalar integrals in dimensional regularization, which was used in our previous work [24,25].

This paper is organized as follows. In Sec. II, we give the LO cross section for the process. The calculation of NLO QCD corrections is described in Sec. III. In Sec. IV, we present the formula in final integration to obtain the transverse momentum distribution of J/ψ production. Section V is devoted to the description about the calculation of J/ψ polarization. The color factor treatment for all the calculated processes are given in Sec. VI. In Sec. VII, treatment of Υ is given. The numerical results are presented in Sec. VIII. Finally, the conclusion and discussion are given in Sec. IX.

II. THE LO CROSS SECTION OF J/ψ HADRONPRODUCTION

The related Feynman diagrams which contribute to the LO amplitude of the partonic process $g(p_1) + g(p_2) \to J/\psi(p_3) + g(p_4)$ are shown in Fig. 1, while the others can be obtained by permuting the places of gluons.

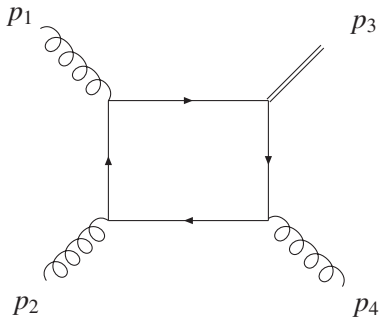

FIG. 1. Leading-order Feynman diagrams for $g + g \to J/\psi + g$. The other five diagrams can be obtained by permutation of the places of gluons.

In the nonrelativistic limit, we can use the NRQCD factorization formalism to obtain the partonic differential cross section in $n = 4 - 2\epsilon$ dimensions as

$$\frac{d\hat{\sigma}^B}{d\hat{t}} = \frac{5\pi\alpha_s^3 |R_s(0)|^2 [\hat{s}^2(\hat{s}-1)^2 + \hat{t}^2(\hat{t}-1)^2 + \hat{u}^2(\hat{u}-1)^2]}{144 m_c^5 \hat{s}^2(\hat{s}-1)^2(\hat{t}-1)^2(\hat{u}-1)^2} + \mathcal{O}(\epsilon), \quad (1)$$

by introducing three dimensionless kinematic variables:

$$\hat{s} = \frac{(p_1+p_2)^2}{4m_c^2}, \quad \hat{t} = \frac{(p_1-p_3)^2}{4m_c^2}, \quad \hat{u} = \frac{(p_1-p_4)^2}{4m_c^2}, \quad (2)$$

where $R_s(0)$ is the radial wave function at the origin of J/ψ and the reasonable approximation $M_{J/\psi} = 2m_c$ is taken.

The LO total cross section is obtained by convoluting the partonic cross section with the parton distribution function (PDF) $G_g(x, \mu_f)$ in the proton:

$$\sigma^B = \int dx_1 dx_2 G_g(x_1, \mu_f) G_g(x_2, \mu_f) \hat{\sigma}^B, \quad (3)$$

where μ_f is the factorization scale. In the following $\hat{\sigma}$ represents the corresponding partonic cross section.

III. THE NLO CROSS SECTION OF J/ψ HADRONPRODUCTION

The NLO contributions to the process can be written as a sum of two parts: one is the virtual correction which arises from loop diagrams, the other is the real correction caused by radiation of a real gluon, or a gluon splitting into a light quark-antiquark pair, or a light (anti)quark splitting into a light (anti)quark and a gluon.

A. Virtual corrections

There are UV, IR, and Coulomb singularities in the calculation of the virtual corrections. UV-divergences existing in the self-energy and triangle diagrams are removed by the renormalization of the QCD gauge coupling constant, the charm quark mass, charm quark field, and gluon field. Here we adopt the renormalization scheme used in Ref. [40]. For the charm quark mass, charm quark field, and gluon field, the renormalization constant Z_m, Z_2, and Z_3 are determined in the on-mass-shell (OS) scheme while for the QCD gauge coupling constant, Z_g is fixed in the modified-minimal-subtraction($\overline{\text{MS}}$) scheme:

$$\delta Z_m^{\rm OS} = -3C_F\frac{\alpha_s}{4\pi}\left[\frac{1}{\epsilon_{\rm UV}} - \gamma_E + \ln\frac{4\pi\mu_r^2}{m_c^2} + \frac{4}{3}\right],$$
$$\delta Z_2^{\rm OS} = -C_F\frac{\alpha_s}{4\pi}\left[\frac{1}{\epsilon_{\rm UV}} + \frac{2}{\epsilon_{\rm IR}} - 3\gamma_E + 3\ln\frac{4\pi\mu_r^2}{m_c^2} + 4\right],$$
$$\delta Z_3^{\rm OS} = \frac{\alpha_s}{4\pi}\left[(\beta_0 - 2C_A)\left(\frac{1}{\epsilon_{\rm UV}} - \frac{1}{\epsilon_{\rm IR}}\right)\right],$$
$$\delta Z_g^{\overline{\rm MS}} = -\frac{\beta_0}{2}\frac{\alpha_s}{4\pi}\left[\frac{1}{\epsilon_{\rm UV}} - \gamma_E + \ln(4\pi)\right], \quad (4)$$

where γ_E is Euler's constant, $\beta_0 = \frac{11}{3}C_A - \frac{4}{3}T_F n_f$ is the one-loop coefficient of the QCD beta function, and n_f is the number of active quark flavors. There are three massless light quarks u, d, s, so $n_f = 3$. In $SU(3)_c$, color factors are given by $T_F = \frac{1}{2}$, $C_F = \frac{4}{3}$, $C_A = 3$. And μ_r is the renormalization scale.

After having fixed the renormalization scheme, there are 129 NLO diagrams in total, including counter-term diagrams. They are shown in Fig. 2, and divided into eight groups. Diagrams of Fig. 2(e) that has a virtual gluon line connected with the quark pair lead to Coulomb singularity, which can be isolated by introducing a small relative velocity $v = |\vec{p}_c - \vec{p}_{\bar{c}}|$. The corresponding contribution is also of $\mathcal{O}(\alpha_s)$ and can be mapped into the $c\bar{c}$ wave function.

$$\sigma = |R_s(0)|^2\hat{\sigma}^{(0)}\left(1 + \frac{\alpha_s}{\pi}C_F\frac{\pi^2}{v} + \frac{\alpha_s}{\pi}C + \mathcal{O}(\alpha_s^2)\right)$$
$$\Rightarrow |R_s^{\rm ren}(0)|^2\hat{\sigma}^{(0)}\left[1 + \frac{\alpha_s}{\pi}C + \mathcal{O}(\alpha_s^2)\right]. \quad (5)$$

The Passarino-Veltman reduction [41] is adopted in the tensor decomposition when its Gram determinant is nonzero. Otherwise, we do the integration directly with Feynman parametrization for the two-point tensor case; and for other cases, we write the Lorentz structure with independent external momentums and apply the Passarino-Veltman reduction again. In the calculation of the scalar integral, we first try to decompose the scalar integral into several lower-point ones when its Gram determinant is zero; if it fails, then we do the integration directly with the Feynman parametrization just like the treatment to the scalar integral with nonzero Gram determinants. The above procedure, including both reduction and integration, is done by FDC automatically.

In our calculation, there is a total of 86 scalar integrals:

(i) Sixty-five of the total 86 integrals, can be found in Ref. [7] after including the permutation of $\hat{s}$, $\hat{t}$, and $\hat{u}$. But the explicit results for the three Coulomb singular five-point scalar integrals is not available in Ref. [7].

(ii) The remaining 21 integrals are not listed in Ref. [7]. Twelve of them can be reduced to a combination of some lower-point scalar integrals and needn't be integrated directly.

(iii) Another six of them can be expressed by the following two integrals, $C(p_1, p_3, m_c, m_c, m_c)$ and $D(p_1, p_4, p_3 + p_4, 0, m_c, m_c, m_c)$, through permutation of $\hat{s}$, $\hat{t}$, and $\hat{u}$, where A, B, C, D, E are defined exactly the same as in Ref. [7]. They can be written into a linear combination of another two scalar in-

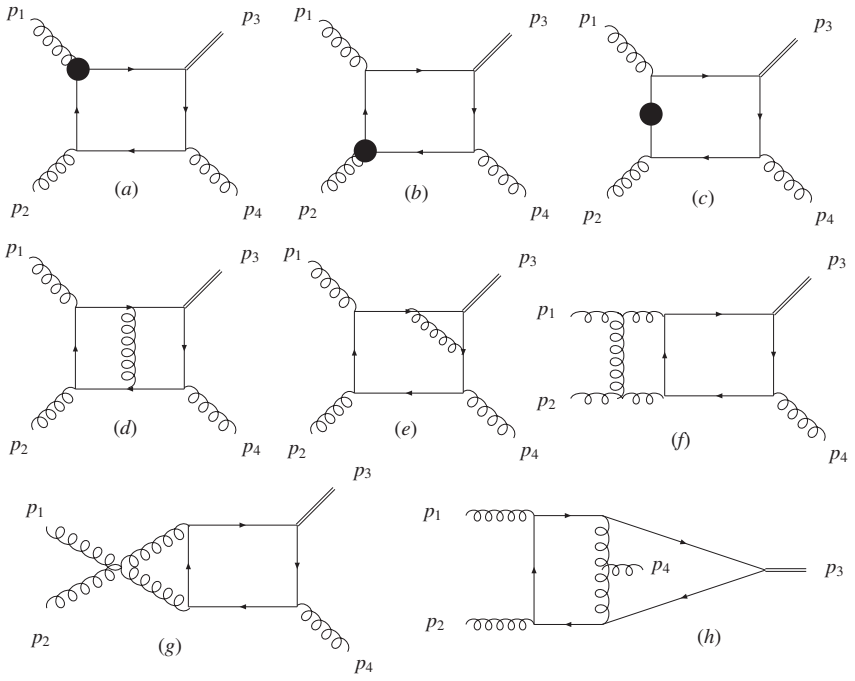

FIG. 2. One-loop diagrams for $gg \to J/\psi g$. Group (a) and (b) are counter-term diagrams of the quark-gluon vertex and corresponding loop diagrams; Group (c) are the quark self-energy diagrams and corresponding counter-term ones. More diagrams can be obtained by permutation of external gluons.

tegrals as

$$C(p_1, p_3, m_c, m_c, m_c) = \frac{1}{2}C(-p_3/2, -p_3/2 + p_1, 0, m_c, m_c) + \frac{1}{2}C(p_3/2, -p_3/2 + p_1, 0, m_c, m_c),$$
$$D(p_1, p_4, p_3 + p_4, 0, m_c, m_c, m_c) = \frac{1}{2}D(p_3/2, p_3/2 - p_2, -p_3/2 - p_4, m_c, m_c, m_c, m_c) + \frac{1}{2}D(-p_3/2, p_3/2 - p_2, -p_3/2 - p_4, m_c, m_c, m_c, m_c). \quad (6)$$

But in our calculation, they are calculated independently, and the above relationship can be used to check all three scalar integrals.

(iv) The remaining three scalar integrals can be expressed by $B(p_1, m_c, m_c)$ through the permutation of $\hat{s}$, $\hat{t}$, and $\hat{u}$.

More details about these 86 scalar integrals can be found at the FDC homepage [42].

By adding all the diagrams together, the virtual corrections to the differential cross section can be expressed as

$$\frac{d\hat{\sigma}^V}{dt} \propto 2\,\mathrm{Re}(M^B M^{V*}), \quad (7)$$

where M^B is the amplitude at LO, and M^V is the renormalized amplitude at NLO. M^V is UV and Coulomb finite, but it still contains the IR divergences:

$$M^V|_{\mathrm{IR}} = \left[\frac{\alpha_s}{2\pi}\frac{\Gamma(1-\epsilon)}{\Gamma(1-2\epsilon)}\left(\frac{4\pi\mu_r^2}{s_{12}}\right)^{\epsilon}\right]\left(\frac{A_2^V}{\epsilon^2} + \frac{A_1^V}{\epsilon}\right)M^B, \quad (8)$$

with

$$A_2^V = -\frac{9}{2},$$
$$A_1^V = -\frac{3}{2}\left[\ln\left(\frac{\hat{s}}{-\hat{t}}\right) + \ln\left(\frac{\hat{s}}{-\hat{u}}\right)\right] + \frac{1}{2}n_f - \frac{33}{4}. \quad (9)$$

And the total cross section of virtual contribution could be written as

$$\sigma^V = \int dx_1 dx_2 G_g(x_1, \mu_f) G_g(x_2, \mu_f)\hat{\sigma}^V. \quad (10)$$

B. Real corrections

The real corrections arise from four parton level subprocesses:

$$g(p_1) + g(p_2) \to J/\psi(p_3) + g(p_4) + g(p_5), \quad (11)$$

$$g(p_1) + g(p_2) \to J/\psi(p_3) + q(p_4) + \bar{q}(p_5), \quad (12)$$

$$g(p_1) + q(\bar{q})(p_2) \to J/\psi(p_3) + g(p_4) + q(\bar{q})(p_5), \quad (13)$$

$$g(p_1) + g(p_2) \to J/\psi(p_3) + c(p_4) + \bar{c}(p_5). \quad (14)$$

We have neglected the contribution from a real correction subprocess $q\bar{q} \to J/\psi gg$, which is IR finite and tiny (it only contributes about 0.002% at $p_t = 3$ GeV and 0.05% at $p_t = 50$ GeV to the differential cross section). And Feynman diagrams for the above processes are shown in Figs. 3 and 4. The phase space integration of the above processes (except $gg \to J/\psi + c\bar{c}$) generates IR singularities, which are either soft or collinear and can be conveniently isolated by slicing the phase space into different regions. We use the two-cutoff phase space slicing method [43] to decompose the phase space into three parts by introducing two small cutoffs.

Real gluon emission brings soft singularities. A small soft cutoff δ_s is used to divide the phase space into two regions according to whether the emitted gluon is soft or hard. Then another small cutoff δ_c is used to decompose the hard region into collinear and noncollinear regions. Then the cross section of real correction processes can be written as

$$\sigma^R = \sigma^S + \sigma^{HC} + \sigma^{H\bar{C}}. \quad (15)$$

The hard noncollinear part $\sigma^{H\bar{C}}$ is IR finite and can be numerically computed using standard Monte Carlo integration techniques. The subprocess $gg \to J/\psi + c\bar{c}$ consists of only a hard noncollinear part.

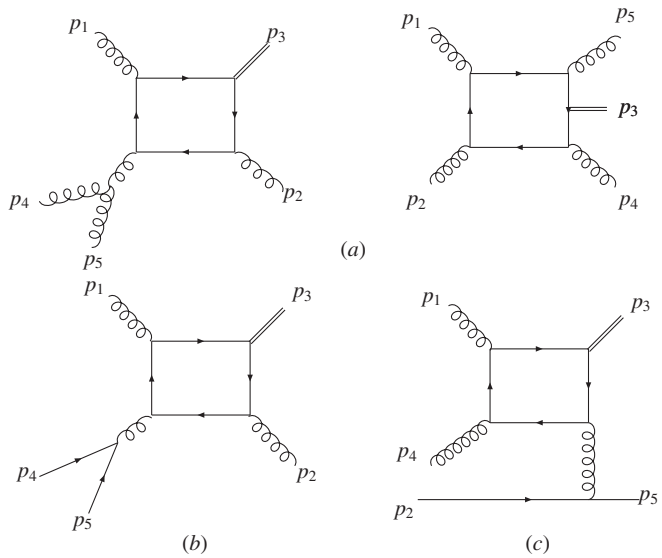

FIG. 3. Feynman diagrams for the first three real correction processes. (a) is for $gg \to J/\psi + gg$ and (b) is for $gg \to J/\psi + q\bar{q}$ while (c) is for $gq(\bar{q}) \to J/\psi + gq(\bar{q})$. More diagrams can be obtained by all possible permutations of gluons.

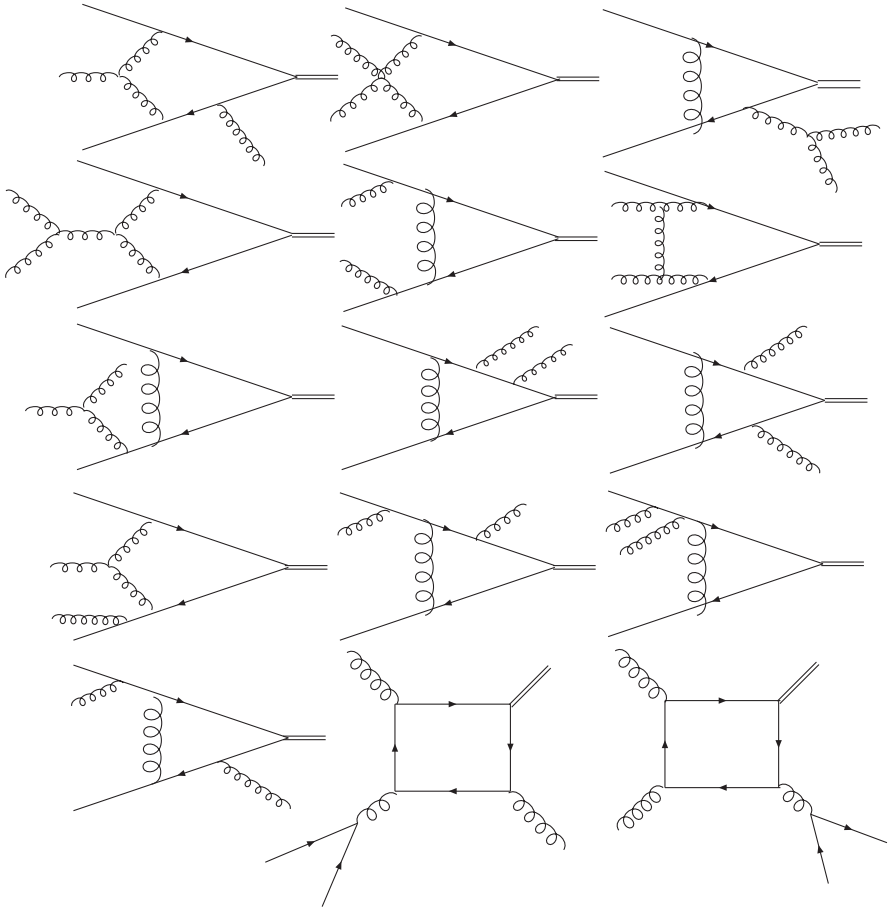

FIG. 4. Feynman diagrams for real correction process $gg \to J/\psi + c\bar{c}$. More diagrams can be obtained by reversing the arrow of the charm quark line and/or exchanging the places of gluons.

1. Soft

It is easy to find that soft singularities caused by emitting soft gluons from the charm quark-antiquark pair in the S-wave color-singlet J/ψ are canceled by each other. Therefore only the real gluon emission subprocess in Eq. (11), where there could be a soft gluon emitted from the external gluons, contains soft singularities. Suppose p_5 is the momentum of the emitted gluon. If we define the Mandelstam invariants as $s_{ij} = (p_i + p_j)^2$ and $t_{ij} = (p_i - p_j)^2$, the soft region is defined in terms of the energy of p_5 in the $p_1 + p_2$ rest frame by $0 \le E_5 \le \delta_s\sqrt{s_{12}}/2$. In this region, soft approximation can be made and the matrix element squared can be factorized as

$$|M_R|^2|_{\text{soft}} \simeq -4\pi\alpha_s\mu_r^{2\epsilon}\sum_{i,j=1,2,4}\frac{-p_i\cdot p_j}{(p_i\cdot p_5)(p_j\cdot p_5)}M_{ij}^0, \tag{16}$$

with

$$M_{ij}^0 = [\mathbf{T}^a(i)\mathbf{M}^B_{b_1\cdots b_{i'}\cdots b_4}]^\dagger[\mathbf{T}^a(j)\mathbf{M}^B_{b_1\cdots b_{j'}\cdots b_4}] \tag{17}$$

and

$$\mathbf{T}^a(j) = if_{ab_jb_{j'}}, \tag{18}$$

where $\mathbf{M}^B_{b_1\cdots b_4}$ is the color connected Born matrix element.

Meanwhile, if we parametrize the emitted gluon's n-dimension momentum in the $p_1 + p_2$ rest frame as

$$p_5 = E_5(1, \ldots, \sin\theta_1\cos\theta_2, \cos\theta_1), \tag{19}$$

the three-body phase space in the soft limit can also be factorized as

$$\mathrm{d}\Gamma_3|_{\text{soft}} = \mathrm{d}\Gamma_2\left[\left(\frac{4\pi}{s_{12}}\right)^\epsilon\frac{\Gamma(1-\epsilon)}{\Gamma(1-2\epsilon)}\frac{1}{2(2\pi)^2}\right]\mathrm{d}S, \tag{20}$$

with

$$\mathrm{d}S = \frac{1}{\pi}\left(\frac{4}{s_{12}}\right)^{-\epsilon} \times \int_0^{\delta_s\sqrt{s_{12}}/2}\mathrm{d}E_5E_5^{1-2\epsilon}\sin^{1-2\epsilon}\theta_1 d\theta_1\sin^{-2\epsilon}\theta_2 d\theta_2, \tag{21}$$

as given in Ref. [43]. After analytical integration over the soft gluon phase space, the parton level cross section in the soft region can be expressed as

$$\hat{\sigma}^S = \hat{\sigma}^B\left[\frac{\alpha_s}{2\pi}\frac{\Gamma(1-\epsilon)}{\Gamma(1-2\epsilon)}\left(\frac{4\pi\mu_r^2}{s_{12}}\right)^{\epsilon}\right]\left(\frac{A_2^S}{\epsilon^2}+\frac{A_1^S}{\epsilon}+A_0^S\right) \tag{22}$$

with

$$A_2^S = 9, \qquad A_1^S = 3\left[\ln\left(\frac{\hat{s}-1}{-\hat{t}}\right)+\ln\left(\frac{\hat{s}-1}{-\hat{u}}\right)\right]-18\ln\delta_s, \tag{23}$$

and

$$\begin{aligned} A_0^S = {} & 18\ln^2\delta_s - 6\ln\delta_s\left[\ln\left(\frac{\hat{s}-1}{-\hat{t}}\right)+\ln\left(\frac{\hat{s}-1}{-\hat{u}}\right)\right] \\ & + \frac{3}{2}\left[\ln^2\left(\frac{\hat{s}-1}{-\hat{t}}\right)+\ln^2\left(\frac{\hat{s}-1}{-\hat{u}}\right)\right] \\ & + 3\left[\mathrm{Li}_2\left(\frac{-\hat{t}}{\hat{s}-1}\right)+\mathrm{Li}_2\left(\frac{-\hat{u}}{\hat{s}-1}\right)\right]. \end{aligned} \tag{24}$$

2. Hard collinear

The hard collinear regions of the phase space are those where any invariant (s_{ij} or t_{ij}) becomes smaller in magnitude than $\delta_c s_{12}$. It is treated according to whether the singularities are from initial or final state emitting or splitting in the origin. The subprocess in Eq. (12) contains final state collinear singularities, and the subprocess in Eq. (13) contains initial state collinear singularities while the subprocess in Eq. (11) contains both.

a. final state collinear. For subprocesses in Eqs. (11) and (12), the final state collinear region is defined by $0 \le s_{45} \le \delta_c s_{12}$. As a consequence of the factorization derivation [44,45], the squared matrix element factorizes into the product of a splitting kernel and the LO squared matrix element as

$$|M_R|^2|_{\mathrm{coll}} \simeq 4\pi\alpha_s\mu_r^{2\epsilon}\frac{2}{s_{45}}P_{44'}(z,\epsilon)|M^B|^2, \tag{25}$$

where $4'$ denotes the parton which splits into parton 4 and 5 collinear pair and $P_{ij}(z,\epsilon)$ are the unregulated ($z<1$) splitting functions in $n=4-2\epsilon$ dimensions related to the usual Altarelli-Parisi splitting kernels [46] with z denoting the fraction of the momentum of parton $4'$ carried by parton 4. For $z<1$ the n-dimensional unregulated splitting functions are written as $P_{ij}(z,\epsilon) = P_{ij}(z) + \epsilon P'_{ij}(z)$ with

$$\begin{aligned} & P_{qq}(z) = C_F\frac{1+z^2}{1-z}, \qquad P'_{qq}(z) = -C_F(1-z), \\ & P_{gg}(z) = 6\left[\frac{z}{1-z}+\frac{1-z}{z}+z(1-z)\right], \qquad P'_{gg}(z) = 0, \\ & P_{qg}(z) = \frac{1}{2}[z^2+(1-z)^2], \qquad P'_{qg}(z) = -z(1-z). \end{aligned} \tag{26}$$

Meanwhile, the three-body phase space in the collinear limit can also be factorized as [43]

$$\mathrm{d}\Gamma_3|_{\mathrm{coll}} = \mathrm{d}\Gamma_2\frac{(4\pi)^{\epsilon}}{16\pi^2\Gamma(1-\epsilon)}\mathrm{d}z\mathrm{d}s_{45}[s_{45}z(1-z)]^{-\epsilon}. \tag{27}$$

Hence after integrations of z and s_{45}, the parton level cross section in the hard final state collinear region can be expressed as

$$\begin{aligned} \hat{\sigma}_f^{HC} = {} & \hat{\sigma}^B\left[\frac{\alpha_s}{2\pi}\frac{\Gamma(1-\epsilon)}{\Gamma(1-2\epsilon)}\left(\frac{4\pi\mu_r^2}{s_{12}}\right)^{\epsilon}\right] \\ & \times\left(\frac{A_1^{g\to gg}+A_1^{g\to q\bar{q}}}{\epsilon}+A_0^{g\to gg}+A_0^{g\to q\bar{q}}\right), \end{aligned} \tag{28}$$

where A_1 and A_0 are

$$\begin{aligned} & A_1^{g\to gg} = 3(11/6+2\ln\delta'_s), \\ & A_0^{g\to gg} = 3[67/18-\pi^2/3-\ln^2\delta'_s-\ln\delta_c(11/6+2\ln\delta'_s)], \\ & A_1^{g\to q\bar{q}} = -n_f/3, \\ & A_0^{g\to q\bar{q}} = n_f/3(\ln\delta_c-5/3), \end{aligned} \tag{29}$$

for subprocesses in Eqs. (11) and (12), and

$$\delta'_s = \frac{s_{12}}{s_{12}+s_{45}-M_{J/\psi}^2} \simeq \frac{\hat{s}}{\hat{s}-1}\delta_s. \tag{30}$$

Thus the total cross section for real correction processes in the hard final state collinear region can be written as

$$\sigma_f^{HC} = \int \mathrm{d}x_1\mathrm{d}x_2 G_g(x_1,\mu_f)G_g(x_2,\mu_f)\hat{\sigma}_f^{HC}. \tag{31}$$

b. initial state collinear. For the subprocess in Eq. (13), the hard initial state collinear region is defined by $0 \le -t_{25} \le \delta_c s_{12}$. However for the subprocess in Eq. (11), the hard initial state collinear region is defined if any of the following conditions are satisfied $0 \le -t_{ij} \le \delta_c s_{12}$, with $i=1,2$ and $j=4,5$. For convenience, suppose that 2 and 5 are the partons involved in the splitting $2 \to 2' + 5$ while $2'$ denotes an internal gluon. As in the final state collinear case, the squared matrix element can be written as

$$|M_R|^2|_{\mathrm{coll}} \simeq 4\pi\alpha_s\mu_r^{2\epsilon}\frac{2}{-zt_{25}}P_{2'2}(z,\epsilon)|M^B|^2, \tag{32}$$

where z denotes the fraction of parton 2's momentum carried by parton $2'$ with parton 5 taking a fraction $(1-z)$. And the three-body phase space in the collinear limit can also be factorized as:

$$\mathrm{d}\Gamma_3|_{\mathrm{coll}} = \mathrm{d}\Gamma_2\frac{(4\pi)^{\epsilon}}{16\pi^2\Gamma(1-\epsilon)}\mathrm{d}z\mathrm{d}t_{25}[-(1-z)t_{25}]^{-\epsilon}. \tag{33}$$

The t_{25} integration yields

$$\int_0^{\delta_c s_{12}} -\mathrm{d}t_{25}(-t_{25})^{-1-\epsilon} = -\frac{1}{\epsilon}(\delta_c s_{12})^{-\epsilon}. \tag{34}$$

If we write the total cross section of LO as

$$\mathrm{d}\sigma^B = \mathrm{d}x_1\mathrm{d}x_2 G_g(x_1)G_g(x_2)\mathrm{d}\hat{\sigma}^B, \tag{35}$$

where $G_g(x_i)$ is the bare PDF, and using the above results, the three-body cross section in the hard initial state collinear region can be written as [43]

$$\mathrm{d}\sigma_i^{HC} = G_g(x_1)G_2(y)\mathrm{d}y\mathrm{d}\hat{\sigma}^B(zs_{12}, t_{13}, t_{14})\left[\frac{\alpha_s}{2\pi}\frac{\Gamma(1-\epsilon)}{\Gamma(1-2\epsilon)}\times\left(\frac{4\pi\mu_r^2}{s_{12}}\right)^{\epsilon}\right]\left(-\frac{1}{\epsilon}\right)\delta_c^{-\epsilon}P_{2'2}(z,\epsilon)\mathrm{d}z(1-z)^{-\epsilon}\times\delta(yz-x_2)\mathrm{d}x_1\mathrm{d}x_2. \tag{36}$$

Notice that a factor of $1/z$ has been absorbed into the flux factor for the two-body subprocess, and the delta function used here ensures that the fraction of the hadron's momentum carried by $2'$ is x_2. It is worth stressing that s_{12} here is related to the square of the overall hadronic center-of-mass energy S as $s_{12} = x_1 y S$, while in the LO process it is $s_{12} = x_1 x_2 S$. From now on, we take the latter definition, so that the replacement $s_{12} \to y s_{12}/x_2$ should be made. After the y integration we have

$$\mathrm{d}\sigma_i^{HC} = G_g(x_1)G_2(x_2/z)\mathrm{d}\hat{\sigma}^B\left[\frac{\alpha_s}{2\pi}\frac{\Gamma(1-\epsilon)}{\Gamma(1-2\epsilon)}\left(\frac{4\pi\mu_r^2}{s_{12}}\right)^{\epsilon}\right]\times\left(-\frac{1}{\epsilon}\right)\delta_c^{-\epsilon}P_{2'2}(z,\epsilon)\frac{dz}{z}\left[\frac{(1-z)}{z}\right]^{-\epsilon}\mathrm{d}x_1\mathrm{d}x_2. \tag{37}$$

When all possible two-to-three subprocesses are considered, there will be several contributions, corresponding to a sum over all possible parton 2s. It can be $2 = g$ followed by $g \to gg$ or $2 = q(\bar{q})$ followed by $q(\bar{q}) \to q(\bar{q})g$. The collinear singularity must be factorized and absorbed into the redefinition of the PDF, which is in general called mass factorization [47]. Here we adopt a scale dependent PDF using the $\overline{\mathrm{MS}}$ convention given by [43]:

$$G_b(x,\mu_f) = G_b(x) + \left(-\frac{1}{\epsilon}\right)\left[\frac{\alpha_s}{2\pi}\frac{\Gamma(1-\epsilon)}{\Gamma(1-2\epsilon)}\left(\frac{4\pi\mu_r^2}{\mu_f^2}\right)^{\epsilon}\right]\times\int_x^1\frac{\mathrm{d}z}{z}P_{bb'}(z)G_{b'}(x/z). \tag{38}$$

Use this definition to replace $G_g(x_2)$ in the LO expression (35) and combine the result with the hard initial collinear contribution (37), then the resulting $\mathcal{O}(\alpha_s)$ expression for the hard initial collinear contribution is [43]

$$\mathrm{d}\sigma_i^{HC} = \mathrm{d}\hat{\sigma}^B\left[\frac{\alpha_s}{2\pi}\frac{\Gamma(1-\epsilon)}{\Gamma(1-2\epsilon)}\left(\frac{4\pi\mu_r^2}{s_{12}}\right)^{\epsilon}\right]\times\left\{G_g(x_1,\mu_f)\tilde{G}_g(x_2,\mu_f) + \left[\frac{A_1^{\mathrm{sc}}(g\to gg)}{\epsilon} + A_0^{\mathrm{sc}}(g\to gg)\right]G_g(x_1,\mu_f)G_g(x_2,\mu_f)\right\}\mathrm{d}x_1\mathrm{d}x_2, \tag{39}$$

with

$$\tilde{G}_c(x,\mu_f) = \sum_{c'}\int_x^{1-\delta_s\delta_{cc'}}\frac{dy}{y}G_{c'}(x/y,\mu_f)\tilde{P}_{cc'}(y), \tag{40}$$

and

$$\tilde{P}_{ij}(y) = P_{ij}(y)\ln\left(\delta_c\frac{1-y}{y}\frac{s_{12}}{\mu_f^2}\right) - P'_{ij}(y). \tag{41}$$

The soft collinear factors A_i^{sc} result from the mismatch in the z integrations. They are given by $A_0^{\mathrm{sc}} = A_1^{\mathrm{sc}}\ln(s_{12}/\mu_f^2)$ and $A_1^{\mathrm{sc}}(g\to gg) = 6\ln\delta_s + (33-2n_f)/6$. For the subprocess in Eq. (13), the light quark (antiquark) can come from either initial hadron, while for the subprocess in Eq. (11), the initial collinear may happen to either of the initial gluons, thus the cross section of hard initial collinear regions can be written as

$$\sigma_i^{HC} = \sigma_{\mathrm{add}}^{HC} + \int\hat{\sigma}_i^{HC}G_g(x_1,\mu_f)G_g(x_2,\mu_f)\mathrm{d}x_1\mathrm{d}x_2, \tag{42}$$

with

$$\sigma_{\mathrm{add}}^{HC} \equiv \int\hat{\sigma}^B\left[\frac{\alpha_s}{2\pi}\frac{\Gamma(1-\epsilon)}{\Gamma(1-2\epsilon)}\left(\frac{4\pi\mu_r^2}{s_{12}}\right)^{\epsilon}\right]\times[G_g(x_1,\mu_f)\tilde{G}_g(x_2,\mu_f) + (x_1\leftrightarrow x_2)]\mathrm{d}x_1\mathrm{d}x_2, \tag{43}$$

and

$$\hat{\sigma}_i^{HC} = 2\hat{\sigma}^B\left[\frac{\alpha_s}{2\pi}\frac{\Gamma(1-\epsilon)}{\Gamma(1-2\epsilon)}\left(\frac{4\pi\mu_r^2}{s_{12}}\right)^{\epsilon}\right]\times\left[\frac{A_1^{\mathrm{sc}}(g\to gg)}{\epsilon} + A_0^{\mathrm{sc}}(g\to gg)\right]. \tag{44}$$

C. Cross section of all NLO contributions

The cross section of real correction processes in hard noncollinear regions could be written as

$$\sigma^{H\bar{C}} = \int\Big[\hat{\sigma}^{H\bar{C}}(gg \to J/\psi + gg) + \sum_{q=u,d,s,c}\hat{\sigma}^{H\bar{C}}(gg \to J/\psi + q\bar{q})\Big]\mathrm{d}x_1\mathrm{d}x_2 G_g(x_1,\mu_f) \times G_g(x_2,\mu_f) + \int\sum_{\alpha=u,d,s,\bar{u},\bar{d},\bar{s}}\hat{\sigma}^{H\bar{C}}(g\alpha \to J/\psi + g\alpha) \times [G_g(x_1,\mu_f)G_\alpha(x_2,\mu_f) + (x_1 \leftrightarrow x_2)]\mathrm{d}x_1\mathrm{d}x_2. \quad (45)$$

Thus the cross section of all real corrections becomes

$$\sigma^R = \sigma^{HC}_{\mathrm{add}} + \sigma^{H\bar{C}} + \int(\hat{\sigma}^S + \hat{\sigma}^{HC}_f + \hat{\sigma}^{HC}_i) \times G_g(x_1,\mu_f)G_g(x_2,\mu_f)\mathrm{d}x_1\mathrm{d}x_2. \quad (46)$$

And the total cross section at NLO is

$$\sigma^{\mathrm{NLO}} = \sigma^{HC}_{\mathrm{add}} + \sigma^{H\bar{C}} + \sigma^{V^+}, \quad (47)$$

with

$$\sigma^{V^+} \equiv \int(\hat{\sigma}^B + \hat{\sigma}^V + \hat{\sigma}^S + \hat{\sigma}^{HC}_f + \hat{\sigma}^{HC}_i) \times G_g(x_1,\mu_f)G_g(x_2,\mu_f)\mathrm{d}x_1\mathrm{d}x_2. \quad (48)$$

It is easy to find that there are no IR singularities in the above expression, for $2A_2^V + A_2^S = 0$ and $2A_1^V + A_1^S + A_1^{g\to gg} + A_1^{g\to q\bar{q}} + 2A_1^{\mathrm{sc}}(g \to gg) = 0$. The apparent logarithmic δ_s and δ_c dependent terms also cancel after numerical integration over the phase space.

IV. TRANSVERSE MOMENTUM DISTRIBUTION

To obtain the transverse momentum distribution of J/ψ, a transformation for integration variable ($\mathrm{d}x_2\mathrm{d}t \to \mathrm{d}p_t\mathrm{d}y$) is introduced. Thus we have

$$\sigma = \int \mathrm{d}x_1\mathrm{d}x_2\mathrm{d}t G_g(x_1,\mu_f)G_g(x_2,\mu_f)\frac{\mathrm{d}\hat{\sigma}}{\mathrm{d}t} = \int J\mathrm{d}x_1\mathrm{d}p_t\mathrm{d}y G_g(x_1,\mu_f)G_g(x_2,\mu_f)\frac{\mathrm{d}\hat{\sigma}}{\mathrm{d}t}, \quad (49)$$

and

$$\frac{\mathrm{d}\sigma}{\mathrm{d}p_t} = \int J\mathrm{d}x_1\mathrm{d}y G_g(x_1,\mu_f)G_g(x_2,\mu_f)\frac{\mathrm{d}\hat{\sigma}}{\mathrm{d}t}, \quad (50)$$

with

$$p_1 = x_1\frac{\sqrt{S}}{2}(1,0,0,1), \qquad p_2 = x_2\frac{\sqrt{S}}{2}(1,0,0,-1),$$
$$m_t = \sqrt{M^2_{J/\psi} + p_t^2}, \qquad p_3 = (m_t\cosh y, p_t, 0, m_t\sinh y),$$
$$x_t = \frac{2m_t}{\sqrt{S}}, \qquad \tau = \frac{m_4^2 - M^2_{J/\psi}}{\sqrt{S}}, \qquad J = \frac{4x_1x_2p_t}{2x_1 - x_te^y},$$
$$x_2 = \frac{2\tau + x_1x_te^{-y}}{2x_1 - x_te^y}, \qquad x_1|_{\min} = \frac{2\tau + x_te^y}{2 - x_te^{-y}}, \quad (51)$$

where $\sqrt{S}$ is the center-of-mass energy of $p\bar{p}(p)$ at the Tevatron or LHC, m_4 is the invariant mass of all the final state particles except J/ψ, and y and p_t are the rapidity and transverse momentum of J/ψ in the laboratory frame, respectively.

V. POLARIZATION

The polarization factor α is defined as

$$\alpha(p_t) = \frac{\mathrm{d}\sigma_T/\mathrm{d}p_t - 2\mathrm{d}\sigma_L/\mathrm{d}p_t}{\mathrm{d}\sigma_T/\mathrm{d}p_t + 2\mathrm{d}\sigma_L/\mathrm{d}p_t}. \quad (52)$$

It represents the measurement of J/ψ polarization as function of J/ψ transverse momentum p_t when calculated at each point in p_t distribution. To calculate $\alpha(p_t)$, the polarization of J/ψ must be explicitly retained in the calculation. The partonic differential cross section for a polarized J/ψ could be expressed as

$$\frac{\mathrm{d}\hat{\sigma}_\lambda}{\mathrm{d}t} = a\epsilon(\lambda)\cdot\epsilon^*(\lambda) + \sum_{i,j=1,2}a_{ij}p_i\cdot\epsilon(\lambda)p_j\cdot\epsilon^*(\lambda), \quad (53)$$

where $\lambda = T_1, T_2, L$. $\epsilon(T_1)$, $\epsilon(T_2)$, $\epsilon(L)$ are the two transverse polarization vectors and the longitudinal polarization one of J/ψ, and the polarizations of all the other particles are summed over in n dimensions. It causes a more difficult tensor reduction path than that with all the polarizations being summed over in the calculation of virtual corrections. It is found that a and a_{ij} are finite when the virtual corrections and real corrections are summed up. Therefore there is no difference in the differential cross section $\mathrm{d}\hat{\sigma}_\lambda/\mathrm{d}t$ whether the polarization of J/ψ is summed over in 4 or n dimensions. Thus we can just treat the polarization vectors of J/ψ in 4 dimensions, and also the spin average factor goes back to 4 dimensions.

To make a cross check, we carry out another calculation. Namely, we calculate the differential cross section $\sigma^{HC}_{\mathrm{add}}$ and σ^{V^+} with the polarizations of all particles being summed up analytically. The results are numerically compared with those obtained without summing up the polarization of J/ψ. Moreover, to check gauge invariance, in the expression we explicitly keep the gluon polarization vector and then replace it by its 4-momentum in the final numerical calculation. Definitely the result must be zero, and our results confirm it. To calculate $\sigma^{H\bar{C}}$, only numerical computation is carried out, and we only sum over the physical polarizations of the gluons to avoid involving diagrams which contain external ghost lines.

VI. COLOR FACTOR

There is just one color factor $d_{c_1c_2c_4}$ for the LO process in the amplitude level with c_1, c_2, and c_4 being the color indices of the three gluons in the process. And it is the same for the virtual correction process that only one color factor

$d_{c_1c_2c_4}$ appears in the amplitude level. For other processes, color factors are orthogonalized and normalized. There are three color factors in the amplitude level for real correction process $g + g \to J/\psi + g + g$:

$$\begin{aligned}
&\frac{1}{\sqrt{5}}\,\mathrm{Tr}[T^{c_4}T^{c_1}T^{c_5}T^{c_2} - T^{c_4}T^{c_2}T^{c_5}T^{c_1}],\\
&\frac{1}{\sqrt{5}}\,\mathrm{Tr}[T^{c_4}T^{c_5}T^{c_1}T^{c_2} - T^{c_4}T^{c_2}T^{c_1}T^{c_5}],\\
&\frac{1}{\sqrt{5}}\,\mathrm{Tr}[T^{c_4}T^{c_1}T^{c_2}T^{c_5} - T^{c_4}T^{c_5}T^{c_2}T^{c_1}],
\end{aligned} \tag{54}$$

where c_i are the color indices of the external gluons. For $g + g \to J/\psi + q + \bar{q}$, there is one color factor

$$\frac{\sqrt{3}}{6\sqrt{5}}[3(T^{c_1}T^{c_2} + T^{c_2}T^{c_1})_{c_4c_5} - \delta_{c_4c_5}\delta_{c_1c_2}], \tag{55}$$

where c_1, c_2 and c_4, c_5 are the color indices of the external gluons and quark pair, respectively. And $g + q \to J/\psi + g + q$ has almost the same color factor as above. For $g + g \to J/\psi + c + \bar{c}$, there are three color factors,

$$\begin{aligned}
&\frac{1}{2\sqrt{66}}[6(T^{c_2}T^{c_1})_{c_4c_5} + \delta_{c_4c_5}\delta_{c_1c_2}],\\
&\frac{1}{2\sqrt{858}}[4(T^{c_2}T^{c_1})_{c_4c_5} - 22(T^{c_1}T^{c_2})_{c_4c_5} - 3\delta_{c_4c_5}\delta_{c_1c_2}],\\
&\frac{3\sqrt{26}}{52\sqrt{15}}[4(T^{c_2}T^{c_1})_{c_4c_5} + 4(T^{c_1}T^{c_2})_{c_4c_5} - 3\delta_{c_4c_5}\delta_{c_1c_2}],
\end{aligned} \tag{56}$$

where c_1, c_2 and c_4, c_5 are the color indices of the external gluons and c quark pair, respectively.

VII. TREATMENT OF Υ

The production mechanism of Υ at the Tevatron and LHC is very similar to that of J/ψ except that color-octet states contribute much less in Υ production according to the experimental data and LO theoretical predictions. We can apply the results of the above calculation to the case of Υ by doing the substitutions:

$$\begin{aligned}
m_c &\leftrightarrow m_b \qquad & M_{J/\psi} &\leftrightarrow M_\Upsilon\\
R_s(0)^{J/\psi} &\leftrightarrow R_s(0)^\Upsilon \qquad & n_f = 3 &\leftrightarrow n_f = 4.
\end{aligned} \tag{57}$$

Note that the charm quark is treated as a light quark as an approximation. It does not coincide with the definition of CTEQ6M PDFs used in the calculation. The mass of heavy quark is not zero in the definition of CTEQ6M PDFs. This approximation can cause a small uncertainty.

VIII. NUMERICAL RESULT

In our numerical calculations, the CTEQ6L1 and CTEQ6M PDFs [48], and the corresponding fitted value for $\alpha_s(M_Z) = 0.130$ and $\alpha_s(M_Z) = 0.118$, are used for LO and NLO predictions, respectively. At NLO, we use α_s in the two-loop formula as

$$\frac{\alpha_s(\mu)}{4\pi} = \frac{1}{\beta_0 \ln(\mu^2/\Lambda^2_{\mathrm{QCD}})} - \frac{\beta_1 \ln\ln(\mu^2/\Lambda^2_{\mathrm{QCD}})}{\beta_0^3 \ln^2(\mu^2/\Lambda^2_{\mathrm{QCD}})}, \tag{58}$$

where $\beta_1 = 34C_A^2/3 - 4(C_F + 5C_A/3)T_F n_f$ is the two-loop coefficient of the QCD beta function. For the heavy-quark mass and the wave function at the origin, $m_c = 1.5$ GeV and $|R_s(0)|^2 = 0.810$ GeV^3 are used for J/ψ, and $m_b = 4.75$ GeV and $|R_s(0)|^2 = 0.479$ GeV^3 are used for Υ. To choose the renormalization scale μ_r and the factorization scale μ_f in the calculations is an important issue, and it causes the uncertainties for the calculation. We choose $\mu = \mu_r = \mu_f = \sqrt{(2m_Q)^2 + p_t^2}$ as the default choice in the calculation with m_Q being m_c and m_b for J/ψ and Υ, respectively. The center-of-mass energies are chosen as 1.96 TeV at the Tevatron and 14 TeV at the LHC. The two phase space cutoffs δ_s and δ_c are chosen as $\delta_s = 10^{-3}$ and $\delta_c = \delta_s/50$ as a default choice. To check the independence of the final results on the two cutoffs, different values of δ_s and δ_c are used, where δ_s can be as small as $\delta_s = 10^{-5}$. And the invariance is observed within the error tolerance of less than 1%.

It is known that the perturbative expansion cannot be applicable to the regions with small transverse momentum and large rapidity of J/ψ or Υ. Therefore, $P_t > 3$ GeV are used for all the calculations. For the rapidity cut at the Tevatron, we choose the same cut condition as the experiments at the Tevatron [32,33]: $|y| < 0.6$ for J/ψ and $|y| < 1.8$ for Υ. To follow the same cut condition used in Ref. [36], we choose $|y| < 3$ for all calculations at the LHC, and another calculation of J/ψ production at the Tevatron. All the cut conditions are explicitly expressed for each result.

The dependences of the total cross section at the renormalization scale μ_r and factorization scale μ_f are presented in Fig. 5. Since the contribution from the subprocess $gg \to J/\psi c\bar{c}$ is less than 10% of the total result at NLO in the whole region of μ, it gives almost the same plot as Fig. 3 in Ref. [36], which does not include the contribution. The results show that the NLO QCD corrections boost the total cross section by a factor of about 2 at the default choice of the scales $\mu = \mu_0 = \sqrt{(2m_c)^2 + p_t^2}$. One can find that the scale dependence at NLO is not improved for J/ψ.

In Figs. 6–8, the p_t distribution of J/ψ and Υ is shown. It is easy to see that the contribution of NLO correction becomes larger as p_t increases, and in the high p_t region, the NLO prediction is 2–3 orders of magnitude larger than the LO one. As already known, the contribution from subprocesses $gg \to J/\psi c\bar{c}$ or $gg \to \Upsilon b\bar{b}$, which is also of $\mathcal{O}(\alpha_s)$, is large at high p_t region. In order to compare with the results in Ref. [36] and also to see how large the contribution is, the result excluding this contribution is

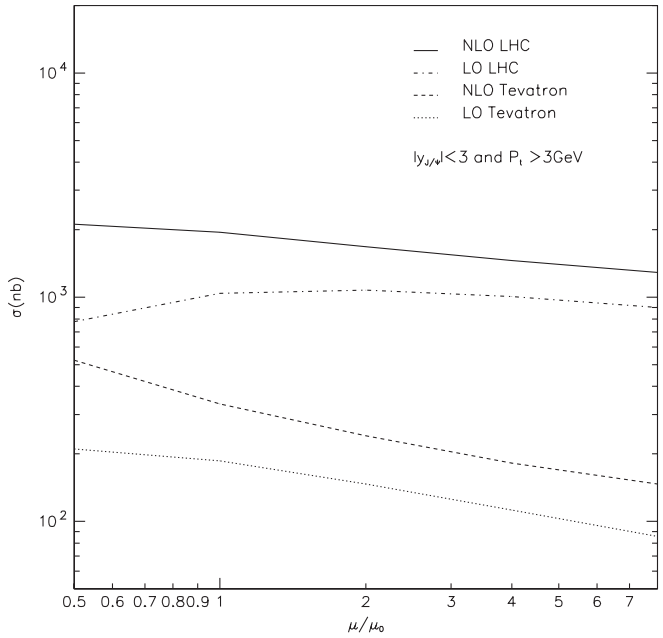

FIG. 5. Total cross section of J/ψ production at the Tevatron and LHC, as function of the renormalization and factorization scale with $\mu_r = \mu_f = \mu$ and $\mu_0 = \sqrt{(2m_c)^2 + p_t^2}$.

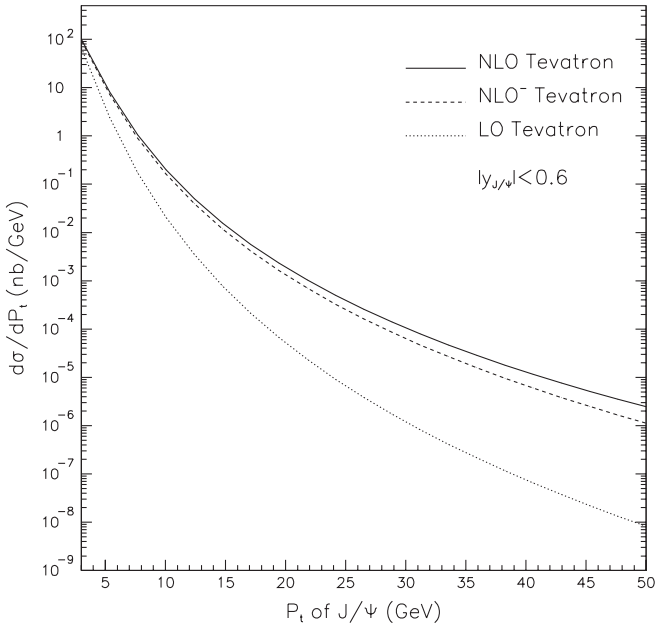

FIG. 7. Transverse momentum distribution of J/ψ production at the Tevatron. NLO$^-$ denotes the result excluding contribution from subprocess $gg \to J/\psi c\bar{c}$.

shown in the figures as NLO$^-$. And we could see from the figures that the contribution from $gg \to \Upsilon b\bar{b}$ in Υ production is less than that from $gg \to J/\psi c\bar{c}$ in the J/ψ case.

The p_t distribution of J/ψ and Υ polarization factor α is presented in Figs. 9 and 10. We can see in the figures that α is always positive and becomes closer to 1 as p_t increases at LO, and this figure means that the transverse polarization is more than the longitudinal one and even becomes dominant in the high p_t region. But there is a dramatic change when the NLO QCD corrections are taken into

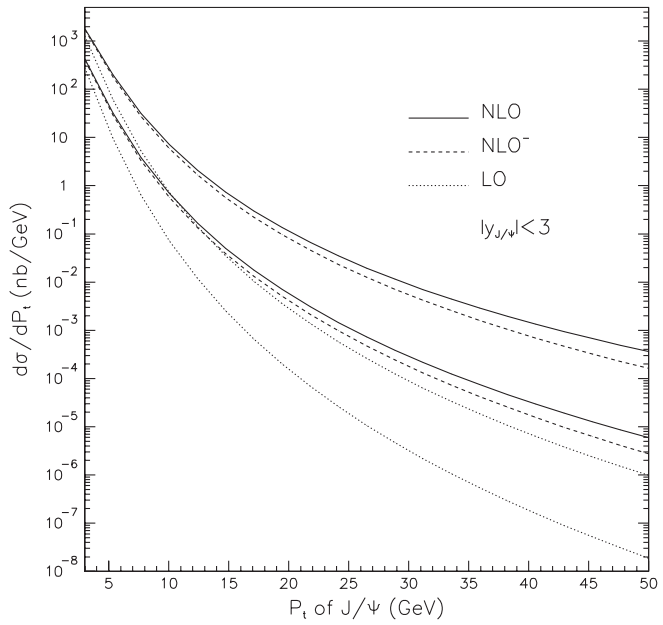

FIG. 6. Transverse momentum distribution of J/ψ production at the LHC (upper curves) and Tevatron (lower curves). NLO$^-$ denotes the result excluding contribution from subprocess $gg \to J/\psi c\bar{c}$.

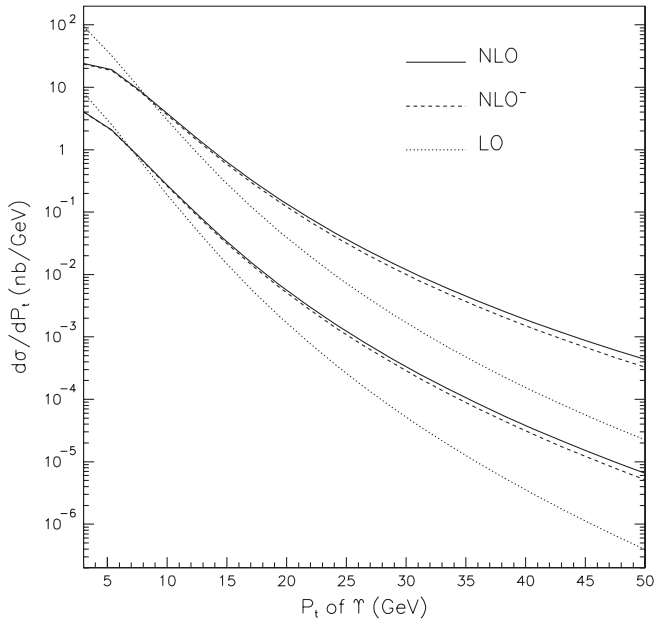

FIG. 8. Transverse momentum distribution of Υ production at the LHC (upper curves) and Tevatron (lower curves). $|y_\Upsilon| < 1.8$ and $|y_\Upsilon| < 3$ are taken for the Tevatron and LHC, respectively. NLO$^-$ denotes the result excluding contribution from subprocess $gg \to \Upsilon b\bar{b}$.

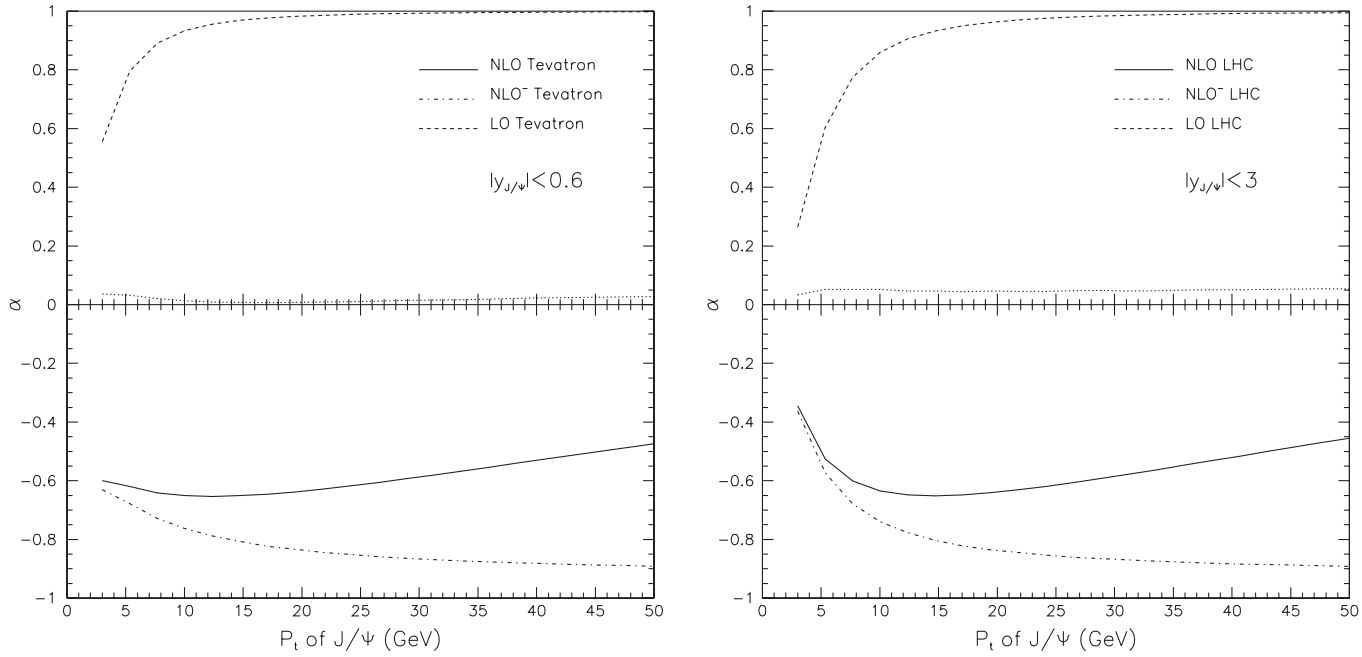

FIG. 9. Transverse momentum distribution of J/ψ polarization at the Tevatron and LHC. NLO$^-$ denotes the result excluding contribution from subprocess $gg \to J/\psi c\bar{c}$, and the process itself is represented by the unlabeled dotted line.

account. For J/ψ, when excluding the contribution from $J/\psi c\bar{c}$, α is always negative and becomes closer to -0.9 as p_t increases; this new figure indicates that the longitudinal polarization is always more than the transverse one and even becomes dominant in the high p_t region. Meanwhile the J/ψ polarization in subprocess $gg \to J/\psi c\bar{c}$ is near zero. By including the contribution of this subprocess, the total result shown in the left diagram of Fig. 9 is closer to the experimental result. For Υ, α varies from positive to negative and becomes closer to -0.6 as p_t increases. The Υ polarization of subprocess $gg \to \Upsilon b\bar{b}$ is also near zero. But from Fig. 10 we can see that this

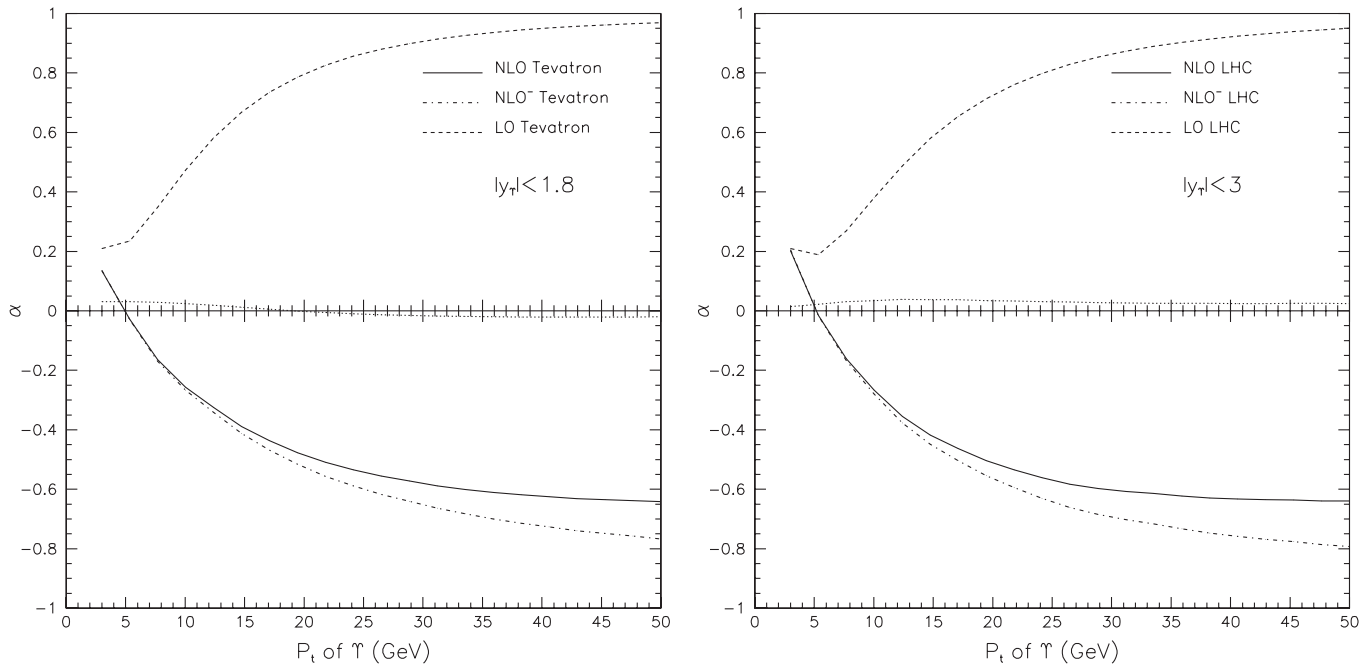

FIG. 10. Transverse momentum distribution of Υ polarization at the Tevatron and LHC. NLO$^-$ denotes the result excluding contribution from subprocess $gg \to \Upsilon b\bar{b}$, and the process itself is represented by the unlabeled dotted line.

TABLE I. Lists of contributions from each channel to the NLO total cross section of J/ψ hadronproduction at the Tevatron in the region $p_t > 3$ GeV and $|y_{J/\psi}| < 3$. We have set $\mu_r = \mu_f = \mu_0$. The corresponding result for σ^B is 1.8682×10^2 nb.

i	Process	$C_0^i(10^2$ nb)	C_0^i/σ^B	Fraction
1	$gg \to J/\psi g$	0.4061 ± 0.0006	0.2174	0.1056
2	$gg \to J/\psi gg$	2.47 ± 0.04	1.32	0.64
3	$gg \to J/\psi q\bar{q}$	0.133 ± 0.001	0.071	0.035
4	$gq \to J/\psi gq$	0.582 ± 0.001	0.312	0.152
5	$gg \to J/\psi c\bar{c}$	0.2583 ± 0.0003	0.1382	0.0672
$\sum$	$p\bar{p} \to J/\psi + X$	3.84 ± 0.04	2.06	1.00

subprocess contributes less than the corresponding one in the case of J/ψ. Also, we find that the contribution from light quarks affects the p_t distribution of polarization less than 10%. When we compare the figures for J/ψ with those for Υ, we can see that they are very similar to each other except that α is higher and even becomes positive in the lower p_t region for Υ. It could be understood by extending the curves for J/ψ to lower p_t, because for a certain p_t value in Υ production, it corresponds to a lower p_t in J/ψ production by just considering the energy scale.

By comparing the experimental measurements for J/ψ [32,49] and for Υ [33,50] at the Tevatron with the above results, we could see that, although NLO corrections can boost the transverse momentum distribution of J/ψ and Υ considerably, it is still an order of magnitude smaller than the experimental data. The color-octet channels are still needed to explain the p_t distribution. Thus the NLO prediction for the polarization of direct J/ψ and Υ via the color-singlet channel could not be used to compare with experimental data.

We can write the contribution of each channel as

$$\sigma^i = C_\epsilon \left(C_2^i \frac{1}{\epsilon^2} + C_1^i \frac{1}{\epsilon} + C_0^i \right) \tag{59}$$

where the overall ϵ dependent factor

$$C_\epsilon = \frac{1}{(1-\epsilon)^2} \left[\frac{4\pi\mu_r^2}{(2m_c)^2} \right]^\epsilon e^{-\epsilon\gamma_E}, \tag{60}$$

and the term $1/(1-\epsilon)^2$ is from the gluon spin average factor $1/(n-2)$. When all the contributions are summed up, we have $\sum C_2^i = 0$ and $\sum C_1^i = 0$. Thus C_ϵ comes back to 1 and we have our result as $\sum C_0^i$. In Table. I, C_0^i is given. Care should be given that the $A_0^{sc}(g \to gg)$ term has been put into the $gg \to J/\psi + gg$ channel even if it contains a term proportional to the number of active flavors n_f.

IX. CONCLUSION AND DISCUSSION

We have calculated the NLO QCD corrections to the J/ψ and Υ hadronproduction at the Tevatron and LHC. Dimensional regularization is applied to deal with the UV and IR singularities in the calculation, and the Coulomb singularity is isolated by a small relative velocity v between the quark pair in the meson and absorbed into the bound state wave function. To deal with the soft and collinear singularities in the real corrections, the two-cutoff phase space slicing method is used. By summing over all the contributions, a result which is UV, IR, and Coulomb finite is obtained.

Numerically, we obtain a K factor of total cross section (ratio of NLO to LO) of about 2 for J/ψ. The transverse momentum distributions of J/ψ and Υ are presented and they show that the NLO corrections increase the differential cross sections more as p_t becomes larger and eventually can enhance it by 2 or 3 orders in magnitude at $p_t = 50$ GeV. This confirms the calculation by Campbell, Maltoni and Tramontano [36]. The real correction subprocesses $gg \to J/\psi c\bar{c}$ and $gg \to \Upsilon b\bar{b}$ are also calculated and the results are in agreement with those of Refs. [16,37].

The NLO contributions to J/ψ polarization are studied, and our results indicate that the J/ψ polarization is dramatically changed from more transverse polarization at LO into more longitudinal polarization at NLO. All the results can be directly applied to ψ' production by multiplying a factor $\langle \mathcal{O}_n^{\psi'} \rangle / \langle \mathcal{O}_n^{\psi} \rangle$. The NLO contributions to Υ polarization are also studied and presented for the first time. Our results indicate that at NLO, the polarization of Υ decreases gradually from near 0.2 to -0.6 as p_t increases from 3 GeV to 50 GeV. Namely, the p_t distribution of the polarization status behaves almost the same as that for J/ψ except that the NLO result is also transverse polarization at small p_t range. Since the fact that contribution via color-octet states is much less in Υ production than that in the J/ψ case, our new result for Υ polarization plays an important role in understanding the experimental data. And even though our calculation results in a more longitudinal polarization state than the recent experimental result for J/ψ [32] and Υ [33] at the Tevatron, it raises a hope to solve the large discrepancy between LO theoretical prediction and experimental measurement on J/ψ and Υ polarization, and suggests that the next important step is to calculate the NLO corrections to hadronproduction of the color-octet state $J/\psi^{(8)}$ and $\Upsilon^{(8)}$. By refixing the color-octet matrix elements, we will see what an involvement of the NLO QCD corrections can induce for the polarization of J/ψ and Υ.

ACKNOWLEDGMENTS

This work was supported by the National Natural Science Foundation of China (No. 10475083) and by the Chinese Academy of Sciences under Project No. KJCX3-SYW-N2.

[1] J. H. Kühn, J. Kaplan, and E. G. O. Safiani, Nucl. Phys. **B157**, 125 (1979); C. H. Chang, Nucl. Phys. **B172**, 425 (1980); B. Guberina, J. H. Kühn, R. D. Peccei, and R. Rückl, Nucl. Phys. **B174**, 317 (1980); E. L. Berger and D. Jones, Phys. Rev. D **23**, 1521 (1981); R. Baier and R. Rückl, Z. Phys. C **19**, 251 (1983).

[2] F. Abe *et al.* (CDF Collaboration), Phys. Rev. Lett. **69**, 3704 (1992); **79**, 572 (1997); **79**, 578 (1997).

[3] E. Braaten and S. Fleming, Phys. Rev. Lett. **74**, 3327 (1995).

[4] G. T. Bodwin, E. Braaten, and G. P. Lepage, Phys. Rev. D **51**, 1125 (1995).

[5] B. A. Kniehl and G. Kramer, Phys. Lett. B **413**, 416 (1997).

[6] P. Ko, J. Lee, and H. S. Song, Phys. Rev. D **54**, 4312 (1996).

[7] M. Kramer, Nucl. Phys. **B459**, 3 (1996).

[8] M. Kramer, J. Zunft, J. Steegborn, and P. M. Zerwas, Phys. Lett. B **348**, 657 (1995).

[9] J. Amundson, S. Fleming, and I. Maksymyk, Phys. Rev. D **56**, 5844 (1997).

[10] M. Cacciari and M. Kramer, Phys. Rev. Lett. **76**, 4128 (1996).

[11] M. Kramer, Prog. Part. Nucl. Phys. **47**, 141 (2001); J. P. Lansberg, Int. J. Mod. Phys. A **21**, 3857 (2006).

[12] H1 Collaboration, in *International Europhysics Conference on High Energy Physics (EPS99), Tampere, Finland, 1999.*

[13] ZEUS Collaboration, in *International Conference on High Energy Physics (ICHEP2000), Osaka, Japan, 2000.*

[14] M. Klasen, B. A. Kniehl, L. N. Mihaila, and M. Steinhauser, Phys. Rev. Lett. **89**, 032001 (2002).

[15] W. de Boer and C. Sander, Phys. Lett. B **585**, 276 (2004).

[16] C.-F. Qiao and J.-X. Wang, Phys. Rev. D **69**, 014015 (2004).

[17] K. Hagiwara, W. Qi, C. F. Qiao, and J. X. Wang, arXiv:0705.0803.

[18] E. Braaten and J. Lee, Phys. Rev. D **67**, 054007 (2003).

[19] K.-Y. Liu, Z.-G. He, and K.-T. Chao, Phys. Lett. B **557**, 45 (2003).

[20] K. Hagiwara, E. Kou, and C.-F. Qiao, Phys. Lett. B **570**, 39 (2003).

[21] K. Abe *et al.* (Belle Collaboration), Phys. Rev. Lett. **89**, 142001 (2002).

[22] B. Aubert *et al.* (*BABAR* Collaboration), Phys. Rev. D **72**, 031101 (2005).

[23] Y.-J. Zhang, Y.-j. Gao, and K.-T. Chao, Phys. Rev. Lett. **96**, 092001 (2006).

[24] B. Gong and J.-X. Wang, Phys. Rev. D **77**, 054028 (2008).

[25] B. Gong and J.-X. Wang, Phys. Rev. Lett. **100**, 181803 (2008).

[26] Z.-G. He, Y. Fan, and K.-T. Chao, Phys. Rev. D **75**, 074011 (2007).

[27] Y.-J. Zhang and K.-T. Chao, Phys. Rev. Lett. **98**, 092003 (2007).

[28] Y.-J. Zhang, Y.-Q. Ma, and K.-T. Chao, Phys. Rev. D **78**, 054006 (2008).

[29] M. Beneke and I. Z. Rothstein, Phys. Lett. B **372**, 157 (1996); **389**, 769(E) (1996); M. Beneke and M. Krämer, Phys. Rev. D **55**, R5269 (1997).

[30] E. Braaten, B. A. Kniehl, and J. Lee, Phys. Rev. D **62**, 094005 (2000); B. A. Kniehl and J. Lee, Phys. Rev. D **62**, 114027 (2000).

[31] A. K. Leibovich, Phys. Rev. D **56**, 4412 (1997).

[32] A. Abulencia *et al.* (CDF Collaboration), Phys. Rev. Lett. **99**, 132001 (2007).

[33] V. M. Abazov *et al.* (D0 Collaboration), arXiv:0804.2799.

[34] E. Braaten and J. Lee, Phys. Rev. D **63**, 071501 (2001).

[35] H. Haberzettl and J. P. Lansberg, Phys. Rev. Lett. **100**, 032006 (2008).

[36] J. Campbell, F. Maltoni, and F. Tramontano, Phys. Rev. Lett. **98**, 252002 (2007).

[37] P. Artoisenet, J. P. Lansberg, and F. Maltoni, Phys. Lett. B **653**, 60 (2007).

[38] B. Gong and J.-X. Wang, Phys. Rev. Lett. **100**, 232001 (2008).

[39] J.-X. Wang, Nucl. Instrum. Methods Phys. Res., Sect. A **534**, 241 (2004).

[40] M. Klasen, B. A. Kniehl, L. N. Mihaila, and M. Steinhauser, Nucl. Phys. **B713**, 487 (2005).

[41] G. Passarino and M. J. G. Veltman, Nucl. Phys. **B160**, 151 (1979).

[42] http://www.ihep.ac.cn/lunwen/wjx/public_html/2008/gggjpsi/index.html.

[43] B. W. Harris and J. F. Owens, Phys. Rev. D **65**, 094032 (2002).

[44] J. C. Collins, D. E. Soper, and G. Sterman, Nucl. Phys. **B261**, 104 (1985).

[45] G. T. Bodwin, Phys. Rev. D **31**, 2616 (1985).

[46] G. Altarelli and G. Parisi, Nucl. Phys. **B126**, 298 (1977).

[47] G. Altarelli, R. K. Ellis, and G. Martinelli, Nucl. Phys. **B157**, 461 (1979).

[48] J. Pumplin, D. R. Stump, J. Huston, H. L. Lai, P. Nadolsky, and W. K. Tung, J. High Energy Phys. 07 (2002) 012.

[49] A. Abulencia *et al.* (CDF Collaboration), Phys. Rev. D **71**, 032001 (2005).

[50] D. E. Acosta *et al.* (CDF Collaboration), Phys. Rev. Lett. **88**, 161802 (2002).